Applied Catalysis B: Environmental 90 (2009) 570–577

Contents lists available at ScienceDirect

Applied Catalysis B: Environmental

journal homepage: www.elsevier.com/locate/apcatb

Al-MCM-41 supported palladium catalyst for methane combustion: Effect of the preparation methodologies

Zhou-jun Wang [a,1], Yuan Liu [a], Peng Shi [a], Chang-jun Liu [a,*], Yan Liu [b]

[a] Key Laboratory for Green Chemical Technology of Ministry of Education, School of Chemical Engineering and Technology, Tianjin University, Tianjin 300072, China
[b] Key Laboratory of Surface and Interface Chemistry of Jilin Province, College of Chemistry, Jilin University, Changchun 130012, China

ARTICLE INFO

Article history:
Received 5 February 2009
Received in revised form 30 March 2009
Accepted 10 April 2009
Available online 17 April 2009

Keywords:
Catalytic combustion
Methane
Palladium
MCM-41
Plasma

ABSTRACT

This work aimed at elucidating the beneficial effect of plasma treatment on the catalytic performance of palladium (Pd) catalysts in methane combustion with the ordered mesoporous molecular sieve Al-MCM-41 as the model support. The plasma treated Pd/Al-MCM-41 catalyst exhibited a higher initial activity and a better stability in comparison with the untreated counterpart catalyst. To clarify the plasma effect, the catalysts were characterized by N_2 sorption analysis, X-ray diffraction (XRD), temperature-programmed desorption of ammonia (NH_3-TPD), pyridine adsorption-infrared spectroscopy (Py-IR), high resolution-transmission electron microscopy (HR-TEM), X-ray photoelectron spectroscopy (XPS) and temperature-programmed reduction (CH_4-TPR) experiments. The results obtained confirmed that palladium oxide (PdO) was the active phase. Plasma treatment enhanced the acidity of catalyst and improved the dispersion of PdO particles, which lead to a higher initial activity. The better stability for plasma treated Pd-based catalyst was proved to be closely related to the stronger interaction between palladium oxide and the molecular sieve support. In addition, the sintering of PdO particles over the plasma treated catalyst was not significant during the stability test. These findings may provide useful guidelines for further catalyst design for methane combustion.

1. Introduction

Catalytic combustion of methane has received considerable attention in the last decades due to its practical applications in both power generation and pollutant abatement [1–4]. This reaction has been shown to be effective in producing energy in gas turbine combustors. Compared to the conventional thermal combustion process, using a heterogeneous catalyst can remarkably decrease the reaction temperature, thereby reducing the noxious emissions of nitrogen oxides [5,6]. Another important application of this reaction is the elimination of trace methane emissions from natural gas or methane combustion devices, as methane is a severe greenhouse gas. One practical example of this application is the abatement of methane emission from lean-burn natural gas vehicles [7].

Pd-based catalysts are renowned for their excellent activity in methane combustion under lean conditions (excess of oxygen) and have been extensively studied in recent years [8–11]. Investigations have shown the catalytic activity to be a complex function of many factors, such as acidity of catalyst, the particle size and morphology of palladium or palladium oxide, state of palladium oxidation. Furthermore, a main problem often encountered was the poor stability, which was usually attributed to sintering of the palladium oxide particles and progressive reduction of palladium oxide clusters. Therefore, in order to develop this reaction as an effective route for energy production, many problems still have to be solved. In particular, a higher activity of the catalyst at low temperature and a better stability under reaction are of prime importance.

Recently, we observed that with the novel glow discharge plasma treatment, the Pd-based catalysts exhibited an enhanced activity and stability in methane combustion compared to the untreated counterpart catalysts [12–14]. Glow discharge, known as a conventional non-thermal plasma, is characterized by high electron temperatures (as high as 10,000–100,000 °C) and low gas temperatures (as low as room temperature). This plasma process is quick, convenient, effective and thus widely applied in the preparation of heterogeneous catalysts and synthesis of nanostructured materials [15,16]. However, the effect of plasma treatment on the catalytic performance of Pd-based catalysts in methane combustion reactions is still unclear and remains a matter under discussion.

* Corresponding author. Tel.: +86 22 27406490; fax: +86 22 27890078.
E-mail address: ughg_cjl@yahoo.com (C.-j. Liu).
[1] Present address: Department of Chemistry, Texas A & M University, College Station, TX 77843-3255, USA.

0926-3373/$ – see front matter © 2009 Elsevier B.V. All rights reserved.
doi:10.1016/j.apcatb.2009.04.012

Herein, we employ the ordered mesoporous molecular sieve Al-MCM-41 as the model support to elucidate how the plasma treatment enhances the initial activity and improves the stability of the Pd-based catalysts in methane combustion. In the past decades, ordered mesoporous molecular sieves have attracted increasing attention in the catalysis field as promising candidates for the catalyst supports owing to their excellent textural properties (high specific surface areas, high pore volumes, narrow pore size distributions, and tunable pore diameters within the nanometer range) [17,18]. Differing from the conventional solid supports (e.g., γ-Al_2O_3, ZrO_2, or amorphous silica, etc.), the ordered mesoporous molecular sieves have the uniform and well-ordered mesopore structures, which makes it possible to obtain much more detailed information from high resolution-transmission electron microscopy (HR-TEM) technique about the dispersion of metal or metal oxide nanoparticles [19]. Compared to other ordered mesoporous molecular sieves (e.g., MCM-41 or SBA-15), the employed Al-MCM-41 model support has another advantage. Brønsted and Lewis acidity are effectively induced by the incorporation of the aluminum into the mesoporous frameworks of MCM-41 silica [20], which is essential for the catalytic activity of Pd-based catalysts in methane combustion. As a matter of fact, the Al-MCM-41 has been reported as the support for methane combustion by Ruiz et al. [21], however, only initial activity data were provided.

In the present work, both the initial activity and stability of PdO/Al-MCM-41 catalyst for methane combustion were investigated. To the best of our knowledge, no study has been reported to date regarding the stability of PdO/Al-MCM-41 catalyst for methane combustion. In order to bring more insight into the beneficial effect induced by plasma treatment, the samples were characterized by N_2 sorption analysis, XRD, NH_3-TPD, Py-IR, HR-TEM, XPS and CH_4-TPR experiments.

2. Experimental

2.1. Catalyst preparation

The preparation of PdO/Al-MCM-41 catalyst includes the following steps: incipient wetness impregnation, drying, glow discharge plasma treatment and thermal calcination.

The Al-MCM-41 (Si/Al = 75) molecular sieve was synthesized according to the method described in the literature [22]. The calcined Al-MCM-41 powder was impregnated with an aqueous solution of $PdCl_2$ (Tianjin Yingda Sparseness & Noble Reagent Chemical Factory, China, 99%) and hydrochloric acid (1 mol/L) for 12 h, followed by drying at 110 °C overnight. Then the resultant sample was treated with argon glow discharge plasma for 45 min.

The glow discharge plasma setup and plasma treatment protocol have been described in detail elsewhere [23,24]. Briefly, the sample (about 0.5 g), loaded on a quartz boat, was placed in the glow discharge cell that was a quartz tube (i.d. 35 mm) with two stainless steel electrodes (o.d. 30 mm). When the pressure in the system was adjusted to 100–200 Pa, the glow discharge plasma was generated by applying 900 V to the electrodes with a 100 Hz square wave using a high voltage amplifier (Trek, 20/20B). The signal input for the high-voltage amplifier was supplied by a function/arbitrary waveform generator (Hewlett-Packard, model 33120A). The current was 4.5 mA. Ultra high pure grade argon (>99.999%) was used as the plasma-forming gas. The temperature of the plasma gas was measured by infrared imaging (Ircon, model 100PHT), indicating that the treatment was conducted at ambient temperature. After plasma treatment, the catalyst was calcined at 500 °C for 4 h. The palladium amount was 1.0 wt%.

For the purpose of comparison, another catalyst was conventionally prepared without the step of glow discharge plasma treatment. In the following sections, the catalyst prepared conventionally was referred as C-PdO/Al-MCM-41 and the catalyst prepared with the plasma treatment was referred as P-PdO/Al-MCM-41.

2.2. Catalytic reaction

The prepared catalysts were evaluated under atmospheric pressure in a fixed-bed horizontal quartz reactor (i.d. 4 mm). In the reactor, the catalyst (100 mg for each test) was held on a quartz wool bed to avoid the generation of hot spots. The temperatures were monitored with a thermocouple, which was located in the center of the catalyst bed. The feed gases containing 1.5 vol.% methane and 6.0 vol.% oxygen in argon were introduced into the catalyst bed at a flow rate of 50 ml/min, corresponding to a gas hourly space velocity (GHSV) of 30,000 ml/(h gcat). The temperature was increased at 5 °C/min from room temperature to the desired reaction temperature in the argon flow (30 ml/min). The effluent gases from the reactor were analyzed with an on-line gas chromatograph (Agilent 4890) equipped with a Porapak Q column. An ice-cold trap was set between the reactor exit and the GC sampling valve to remove the water formed during reaction.

To assess both the initial activity and long-term stability of the prepared catalysts, two different kinds of reaction tests were performed in this work. In the initial activity test, the methane conversion was measured as a function of temperature between 275 and 500 °C with successive heating steps of 25 °C. The methane conversion was collected after 0.5 h duration at each temperature. In the long-term stability test, the catalysts were studied for 48 h with the temperature maintained at 425 °C.

2.3. Catalyst characterizations

2.3.1. Surface areas and porosity

The surface areas and porosity of samples were characterized with N_2 sorption analysis. N_2 adsorption–desorption isotherms were measured at −196 °C on a Micromeritics Tristar 3000 analyzer. Before the measurements, the samples were outgassed at 300 °C for 6 h. The Brumauer–Emmett–Teller (BET) method was employed to calculate the specific surface areas. The pore volumes and pore size distributions were derived from the desorption branches of the isotherms using the Barrett–Joyner–Halanda (BJH) model.

2.3.2. X-ray diffraction (XRD)

The XRD patterns were collected by a Rigaku D/MAX-2500V/PC system using Cu Kα radiation (λ = 0.154056 nm) at 40 kV and 200 mA. The low-angle XRD patterns were collected at a scanning speed of 1°/min over the 2θ range of 0.5–10° while the wide-angle XRD patterns at a scanning speed of 4°/min over the 2θ range of 10–90°.

2.3.3. Acidity measurements

The acidity of samples was analyzed by temperature-programmed desorption of ammonia (NH_3-TPD) and pyridine adsorption-infrared spectroscopy (Py-IR) techniques.

NH_3-TPD test was performed in a Micromeritics 2910 analyzer with the thermal conductivity detector (TCD). After being pretreated at 200 °C under flowing argon (30 ml/min) for 1 h, the sample (75 mg) was cooled to 50 °C, and then adsorbed to saturation by pulses of ammonia for 0.5 h. Physically adsorbed ammonia on catalyst was removed by flushing the sample with argon (30 ml/min) for 1 h at the adsorption temperature. Thermal desorption of ammonia was carried out in the temperature range of 50–500 °C at an increasing temperature rate of 10 °C/min.

Py-IR spectrum was recorded by a Bruker Vector 22 FTIR spectrometer with a resolution of 4 cm^{-1}. 20 mg sample was ground finely, pressed into a self-supporting wafer (diameter of 16 mm) and mounted into a quartz IR cell. Before test, the sample was pretreated by heating up to 400 °C under vacuum and held at this temperature for 1.5 h. Then the temperature of the sample was cooled down to room temperature and pyridine was admitted into the cell until saturation. After that the sample was degassed at 200 °C for 1 h under vacuum and the infrared spectrum was collected at room temperature.

2.3.4. High resolution-transmission electron microscopy (HR-TEM)

The HR-TEM images were recorded on a Philips Tecnai G^2 F20 system operated at 200 kV. The powder sample was sonicated in ethanol for 10 min, dropped and dried on carbon-coated copper grids before test.

2.3.5. X-ray photoelectron spectroscopy (XPS)

The XPS analysis was performed on a Perkin-Elmer PHI-1600 spectrometer with Mg Kα (1253.6 eV) radiation. The binding energy was calibrated by the C 1s peak (284.6 eV) of the surface adventitious carbon.

2.3.6. Temperature-programmed reduction (CH_4-TPR)

The CH_4-TPR was carried out in a flow of 5% CH_4/He mixture gas at a flow rate of 30 ml/min. The sample (about 150 mg) was purged in He gas (30 ml/min) at 200 °C for 1 h to remove physically absorbed impurities on the catalyst surface. Then the catalyst was cooled down to 50 °C and measured by linearly increasing the temperature from 50 to 850 °C at a ramping rate of 10 °C/min. The reduction process was monitored by the consumption of CH_4 with a mass-spectrometer (Pfeiffer Vacuum, GSD301 O2). Methane was identified by the fragmentation pattern at m/e = 15 to avoid the interference of the oxygen fragmentation pattern (at m/e = 16) from CO_2 or water.

3. Results and discussion

3.1. XRD characteristics

The PdO/Al-MCM-41 catalysts, together with the ordered mesoporous molecular sieve Al-MCM-41 model support, were characterized by N_2 adsorption–desorption measurements. Fig. 1 illustrated that the isotherms for Al-MCM-41 and PdO/Al-MCM-41 samples were of type IV with hysteresis loop, which were typical for the regular mesoporous materials [25]. The pore structure parameters for the prepared samples were summarized in Table 1.

Table 1
Specific surface areas, pore volumes, and average pore diameters of Al-MCM-41 support and PdO/Al-MCM-41 catalysts.

Sample	S_{BET} (m^2/g)[a]	V_{BJH} (cm^3/g)[b]	D_{BJH} (nm)[c]
Al-MCM-41	966	0.94	2.8
C-PdO/Al-MCM-41	878	0.84	2.8
P-PdO/Al-MCM-41	878	0.84	2.8

[a] BET specific surface area.
[b] BJH pore volume.
[c] BJH average pore diameter.

The BET surface area of Al-MCM-41 support was quite high, as reported in the literature [26]. After catalyst synthesis, both the BET surface area and volume for the molecular sieve decreased slightly. By comparing the porosity parameters between C-PdO/Al-MCM-41 and P-PdO/Al-MCM-41, we could see that plasma treatment had little influence on the textural properties of the support.

The low-angle XRD was employed to investigate the long-range order of molecular sieve materials. As shown in Fig. 2, all the prepared samples presented a major peak at about 2.2° together with two additional peaks, corresponding to the ordered hexagonal structure in Al-MCM-41 materials. The peak intensities for both C-PdO/Al-MCM-41 and P-PdO/Al-MCM-41 catalysts were not significantly lowered as compared with those of the parent Al-MCM-41, suggesting that the long-range regularity of mesoporous molecular sieve was well maintained during catalyst preparation processes.

3.2. Methane combustion

3.2.1. Investigations of initial activity

The conversion of methane on PdO/Al-MCM-41 as the function of temperature was depicted in Fig. 3 and the data of initial activities were listed in Table 2.

Fig. 3 revealed that both C-PdO/Al-MCM-41 and P-PdO/Al-MCM-41 catalysts exhibited excellent catalytic activities at low temperatures. The methane combustion started at about 275 °C; then the conversion increased drastically with the reaction temperature and the complete conversion was reached at temperatures lower than 475 °C. During the activity tests, CO_2

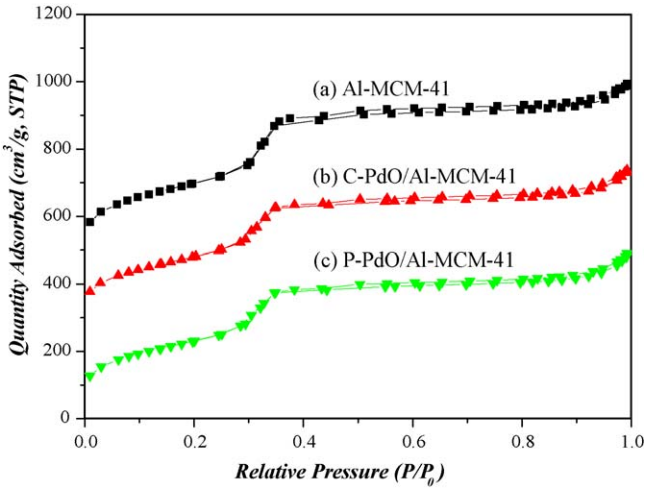

Fig. 1. N_2 adsorption–desorption isotherms of Al-MCM-41 and PdO/Al-MCM-41 samples: (a) Al-MCM-41; (b) C-PdO/Al-MCM-41 and (c) P-PdO/Al-MCM-41.

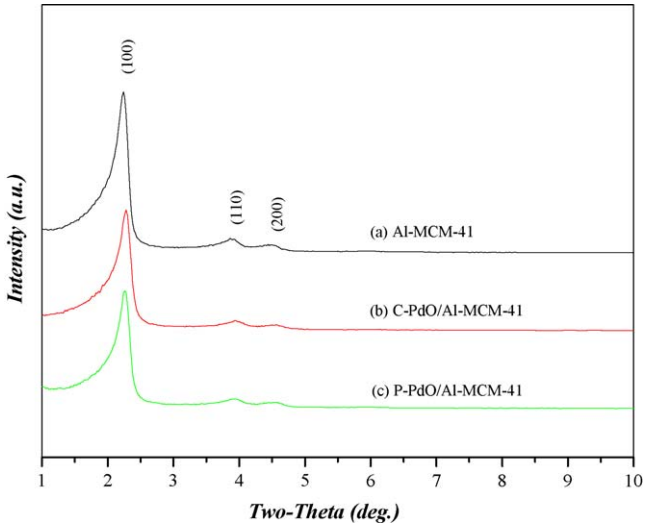

Fig. 2. The low-angle XRD patterns for Al-MCM-41 and PdO/Al-MCM-41 samples: (a) Al-MCM-41; (b) C-PdO/Al-MCM-41 and (c) P-PdO/Al-MCM-41.

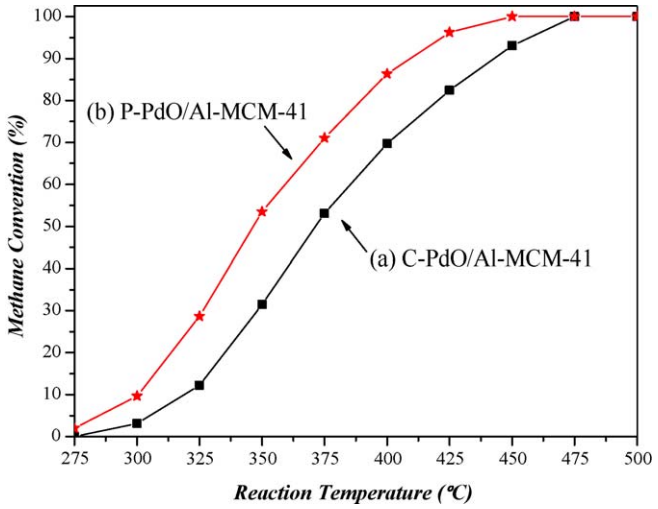

Fig. 3. Initial activity for methane combustion as a function of temperature over PdO/Al-MCM-41 catalysts: (a) C-PdO/Al-MCM-41 and (b) P-PdO/Al-MCM-41. Reaction conditions: the palladium amount = 1.0 wt%; CH_4:O_2:Ar = 1.5:6.0:92.5; GHSV = 30,000 ml/(h gcat).

Table 2
Initial activity of PdO/Al-MCM-41 catalysts on methane combustion reaction (T_{10}, T_{50} and T_{90} represented the reaction temperatures required for 10%, 50% and 90% conversion of CH_4, respectively).

Sample	T_{10} (°C)	T_{50} (°C)	T_{90} (°C)
C-PdO/Al-MCM-41	320	371	443
P-PdO/Al-MCM-41	300	346	409

Reaction conditions: the palladium amount = 1.0 wt%; CH_4:O_2:Ar = 1.5:6.0:92.5; GHSV = 30,000 ml/(h gcat).

was detected as the only carbon-containing reaction product, indicating the complete oxidation of methane.

In comparison, the P-PdO/Al-MCM-41 catalyst displayed higher initial activity than the C-PdO/Al-MCM-41 counterpart. The T_{10}, T_{50} and T_{90} over the P-PdO/Al-MCM-41 reduced by more than 20 °C, as clearly indicated in Table 2.

Furthermore, with the reaction rates normalized as per gram of Pd at a standard temperature (350 °C), the PdO/Al-MCM-41 catalysts in this work could be compared with those in the literature. As summarized in Table 3, the P-PdO/Al-MCM-41 catalyst exhibited a highest activity among the listed Pd-based catalysts. Moreover, each Pd-based catalyst with plasma treatment

Table 3
Normalized reaction rates of Pd-based catalysts for methane combustion at 350 °C.

Catalysts[a]	Preparation methodologies[b]	Reaction rates[c] (mol CH_4/(s g Pd))	Reference
0.98 wt% PdO/Al_2O_3	I	0.0025	[8]
2.0 wt% PdO/Al_2O_3	I	0.0162	[27]
2.0 wt% PdO/Al_2O_3	I + P	0.0670	[27]
0.55 wt% PdO/Al_2O_3	I	0.0068	[28]
0.55 wt% PdO/HZSM-5	I	0.0263	[28]
0.55 wt% PdO/HZSM-5	E	0.0059	[28]
2.0 wt% PdO/HZSM-5	I	0.0284	[12]
2.0 wt% PdO/HZSM-5	I + P	0.112	[12]
1.0 wt% PdO/Al-MCM-41	I	0.632	This work
1.0 wt% PdO/Al-MCM-41	I + P	1.075	This work

[a] The loading refers to the metal amount in the catalyst.
[b] I denotes incipient wetness impregnation; I + P denote incipient wetness impregnation followed by plasma treatment; E denotes ion exchange.
[c] The reaction rates were normalized as per gram of Pd, at a standard temperature (350 °C).

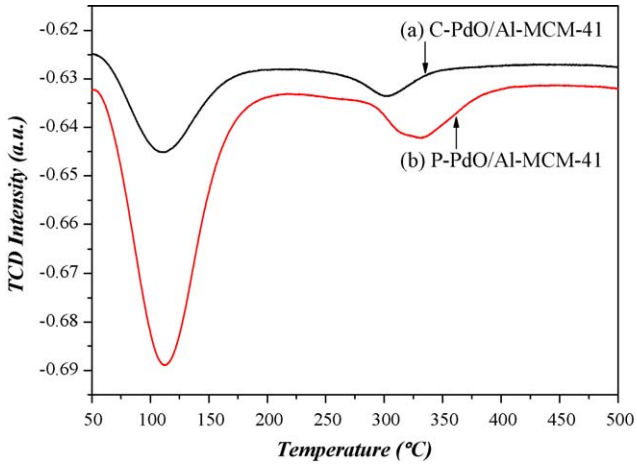

Fig. 4. NH_3-TPD profiles of (a) C-PdO/Al-MCM-41 and (b) P-PdO/Al-MCM-41 catalysts.

possessed a much higher reaction rate than its counterpart with other methodology. These results clearly demonstrated the beneficial effects of the plasma treatment.

It has been pointed out in the literature that the activity of Pd-based catalysts in methane combustion depends strongly on the surface acidity [29], the size of PdO crystallites [28], and the Pd oxidation state [30,31]. Therefore, a series of characterization techniques were carried out to understand how plasma treatment enhanced the initial activity of PdO/Al-MCM-41 catalyst.

The acidity of catalysts was analyzed by NH_3-TPD and Py-IR experiments. It is well-known that, in NH_3-TPD profile, the desorption peak is related to the strength of acid sites while the peak area is related to the number of acid sites [32]. Fig. 4 demonstrated distinctly that there were two kinds of acid sites on the catalysts, weak acid (around 110 °C) and middle strong acid (around 300 °C) sites. Comparatively, the number of acid sites on PdO/Al-MCM-41 catalyst was increased dramatically with the plasma treatment. And the strength of middle strong acid sites was greatly enhanced with an increase of about 30 °C for the peak temperature.

To analyze the type and amount of acid sites on PdO/Al-MCM-41 catalysts, the Py-IR characterization was performed. As shown in Fig. 5, the bands attributed to pyridine adsorbed on Brønsted acid sites (1545 cm^{-1}) and Lewis acid sites (1450 cm^{-1}) were

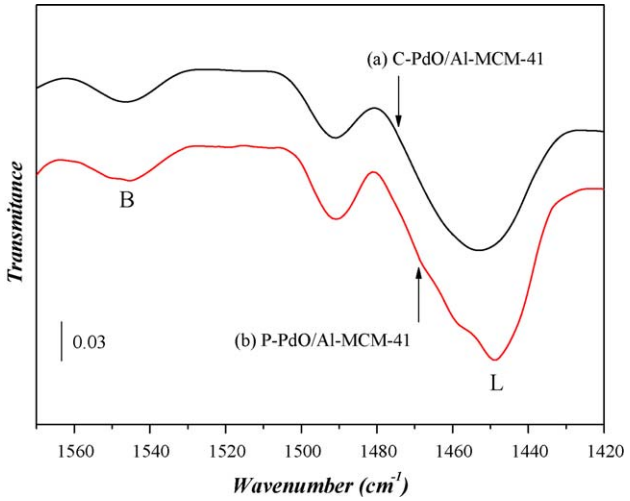

Fig. 5. Py-IR spectra of (a) C-PdO/Al-MCM-41 and (b) P-PdO/Al-MCM-41 catalysts. The bands denoted as B and L are due to pyridine molecules interacting with Brønsted and Lewis acid sites, respectively.

Table 4
The relative amount of acid sites on PdO/Al-MCM-41 catalysts estimated from the integrated areas of each band.

Sample	Brønsted acid sites (a.u.)	Lewis acid sites (a.u.)
C-PdO/Al-MCM-41	0.650	7.189
P-PdO/Al-MCM-41	0.712	10.228

detected. Another band (1490 cm^{-1}) due to pyridine interacting with both Lewis and Brønsted acid sites was also observed [33]. For comparison, the relative amount of acid sites on both C-PdO/Al-MCM-41 and P-PdO/Al-MCM-41 catalysts was estimated from the integrated area of each band. Table 4 demonstrated clearly that plasma treatment increased the amounts of Brønsted acid sites and Lewis acid sites on PdO/Al-MCM-41 catalyst remarkably, which was consistent with the NH_3-TPD results.

As generally agreed, the active phase of Pd catalyst in methane combustion is in the oxidized state, but all the chemisorption techniques employed to characterize dispersions involve reducing treatments. As a consequence, dispersion values measured on the reduced Pd catalyst by chemisorption techniques may not accurately reflect the surface areas of the PdO crystallites present during methane oxidation [34]. To circumvent this experimental difficulty, HR-TEM and XPS techniques are suggested to assess the variations of dispersion for PdO particles [35]. However, the heterogeneity of conventional solid supports makes it cumbersome to obtain detailed information from HR-TEM technique. In this study, with the use of ordered mesoporous Al-MCM-41 as the model support, we can overcome this problem effectively as a clear differentiation can be made between palladium oxide crystallites and ordered mesoporous Al-MCM-41 supports.

Fig. 6 compared the HR-TEM images of different PdO/Al-MCM-41 catalysts. Fig. 6a demonstrated that the PdO particles in C-PdO/Al-MCM-41 catalyst existed as aggregates with an oval or short-rod shape. The length of PdO aggregates varied from 25 to 100 nm. In comparison, the plasma prepared PdO particles (Fig. 6b) were dispersed uniformly on the support with a spherical shape. The average PdO particle size in P-PdO/Al-MCM-41 catalyst was estimated to be 25 nm. This improved dispersion could further be confirmed by the XPS surface analysis.

In this paper, the surface Pd/Al atomic ratio derived from XPS analysis was employed to monitor the dispersion of PdO phase. As displayed in Table 5, the surface Pd/Al ratio for P-PdO/Al-MCM-41 catalyst was much higher than the C-PdO/Al-MCM-41 counterpart, suggesting that the plasma treatment improved the dispersion of PdO particles significantly.

The Pd oxidation state in PdO/Al-MCM-41 catalysts was also confirmed by XPS characterization. As shown in Fig. 7, for

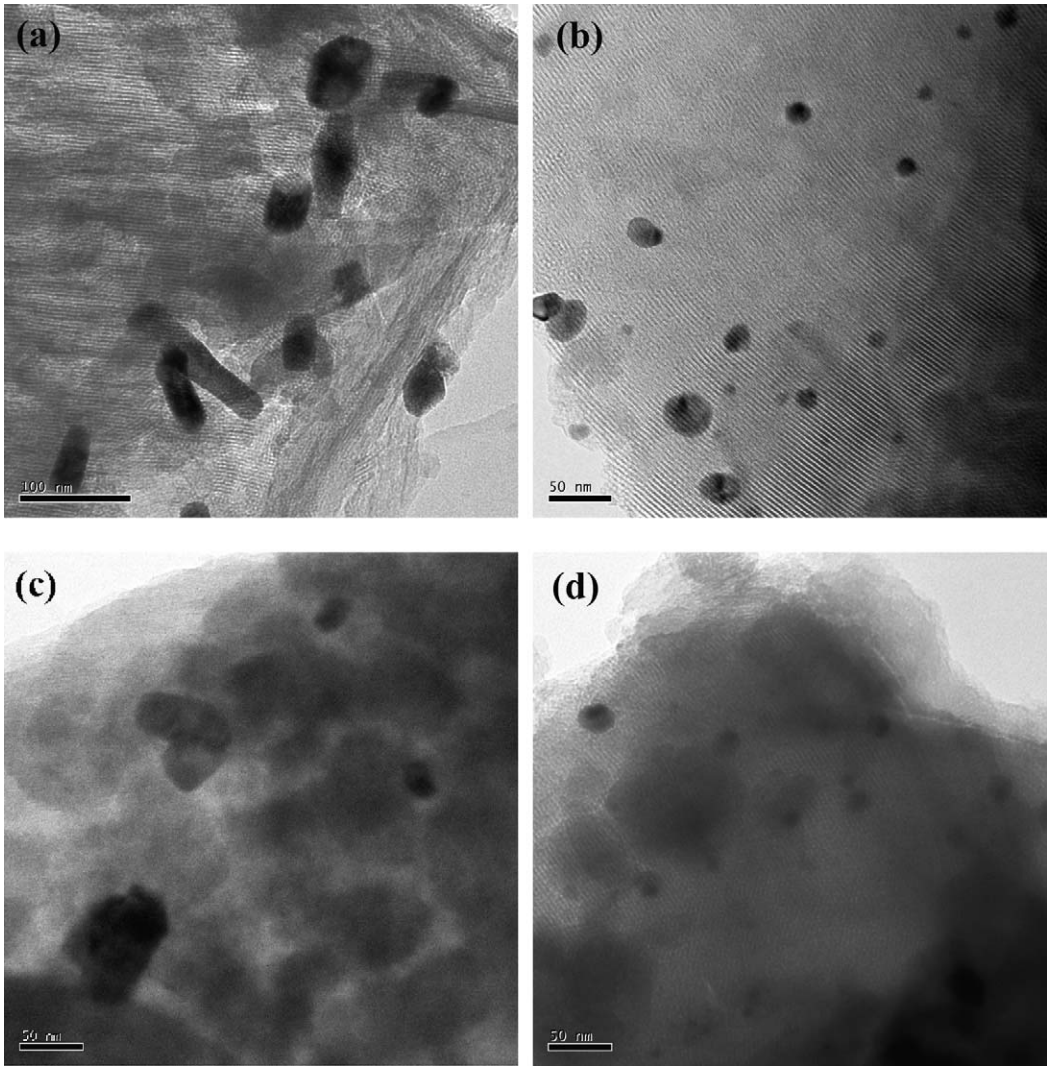

Fig. 6. Typical HR-TEM images for PdO/Al-MCM-41 catalysts: (a) C-PdO/Al-MCM-41 sample before reaction; (b) P-PdO/Al-MCM-41 sample before reaction; (c) C-PdO/Al-MCM-41 sample after 48 h reaction and (d) P-PdO/Al-MCM-41 sample after 48 h reaction.

Table 5
The surface composition of PdO/Al-MCM-41 catalysts derived from XPS analysis.

Sample	Surface atomic composition (%)				Pd/Si (%)
	O	Si	Al	Pd	
C-PdO/Al-MCM-41, before reaction	69.7	29.5	0.7	0.1	0.34
P-PdO/Al-MCM-41, before reaction	69.8	29.4	0.5	0.3	1.02
C-PdO/Al-MCM-41, after 48 h reaction	69.3	29.8	0.8	0.1	0.34
P-PdO/Al-MCM-41, after 48 h reaction	69.3	29.8	0.6	0.3	1.01

both C-PdO/Al-MCM-41 (Fig. 7a) and P-PdO/Al-MCM-41 (Fig. 7b) catalysts, two symmetrical peaks were observed and no other peaks could be deconvoluted. The binding energy of Pd $3d_{5/2}$ in the samples demonstrated that the Pd species were in the state of PdO [36]. Namely, PdO was the active phase in methane combustion.

Summarily, it was confirmed that PdO was the active phase. The beneficial effect of plasma treatment on the initial activity of PdO/Al-MCM-41 catalyst in methane combustion should be ascribed to the enhanced acidity of catalyst and a better PdO dispersion on the support.

3.2.2. Investigations of stability

The stability of PdO/Al-MCM-41 catalysts was evaluated during 48 h under reaction at 425 °C. The evolution of the methane conversion with time on stream was presented in Fig. 8. Both C-PdO/Al-MCM-41 and P-PdO/Al-MCM-41 catalysts showed an initial activation period (<2 h), which was often reported in the literature [37,38]. After the activation period, the activity of C-PdO/Al-MCM-41 catalyst attained at the maximum for ca. 12 h of the elapsed time, and then decreased linearly with time on stream. In contrast, the P-PdO/Al-MCM-41 catalyst showed a much better stability although slight deactivation could also be observed.

The poor stability was a main drawback for the Pd-based catalysts and was extensively investigated in the last decade [39–41]. Amongst the most investigated issues, two main parameters were pointed out as the most relevant ones: sintering of PdO particles [39]; progressive reduction of the palladium oxide clusters [40,41].

The HR-TEM images before (Fig. 6a) and after (Fig. 6c) stability test revealed that the dispersion of PdO particles in the C-PdO/Al-MCM-41 catalyst was well retained during the stability tests. The same conclusion could also be drawn from the XPS data (Table 5). The surface Pd/Si ratio for the C-PdO/Al-MCM-41 catalyst remained constant before and after the stability test, suggesting that the sintering of PdO particles was not significant under reaction. Therefore the deactivation of C-PdO/Al-MCM-41 catalyst in this work should not be ascribed to the sintering of PdO particles. In addition, the HR-TEM images (Fig. 6b and d) together with the XPS results (Table 5) demonstrated that the sintering of PdO particles in P-PdO/Al-MCM-41 catalyst was also negligible.

It was generally accepted that PdO was more active than the metallic Pd [2,7,40–43], which was also confirmed by our studies. Therefore, wide-angle XRD experiments were conducted to examine the palladium phase in the used PdO/Al-MCM-41catalysts (Fig. 9). For the used P-PdO/Al-MCM-41 catalyst, all diffraction peaks were due to PdO phase (JCPDS card, File No. 41-1107). However, for the used C-PdO/Al-MCM-41 catalyst, a small peak at $2\theta = 41.06^\circ$ assigned to Pd (1 1 1) (JCPDS card, File No. 46-1043) could be clearly observed, indicating that the palladium oxide clusters were partially reduced to Pd^0 particles.

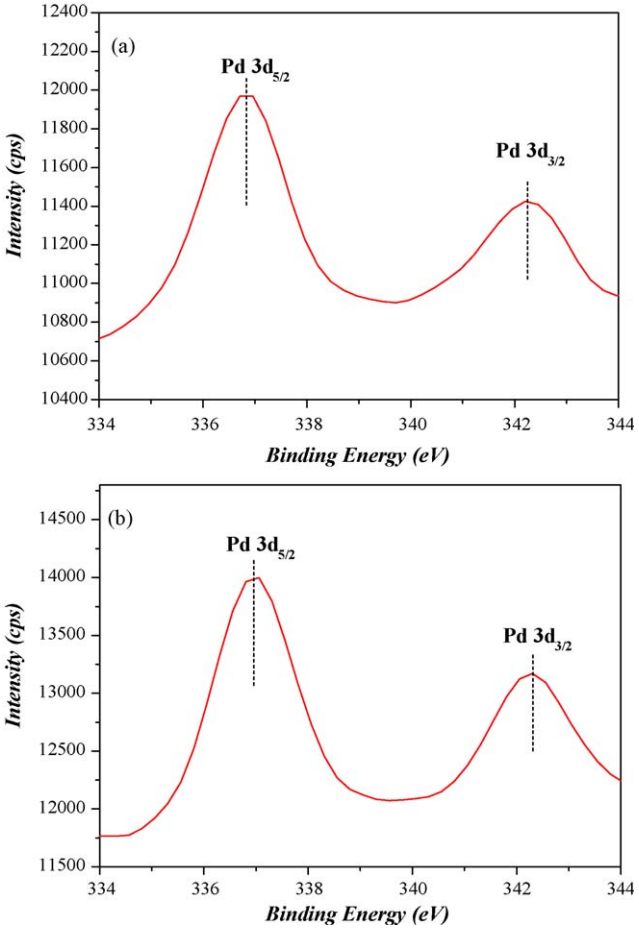

Fig. 7. XPS spectra for (a) C-PdO/Al-MCM-41 and (b) P-PdO/Al-MCM-41 catalysts.

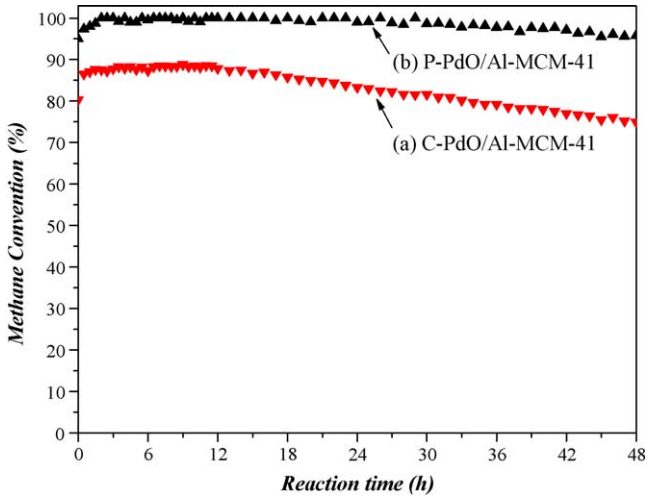

Fig. 8. Stability test of PdO/Al-MCM-41 catalysts for methane combustion at 425 °C: (a) C-PdO/Al-MCM-41 and (b) P-PdO/Al-MCM-41. Reaction conditions: the palladium amount = 1.0 wt%; CH_4:O_2:Ar = 1.5:6.0:92.5; GHSV = 30,000 ml/(h gcat).

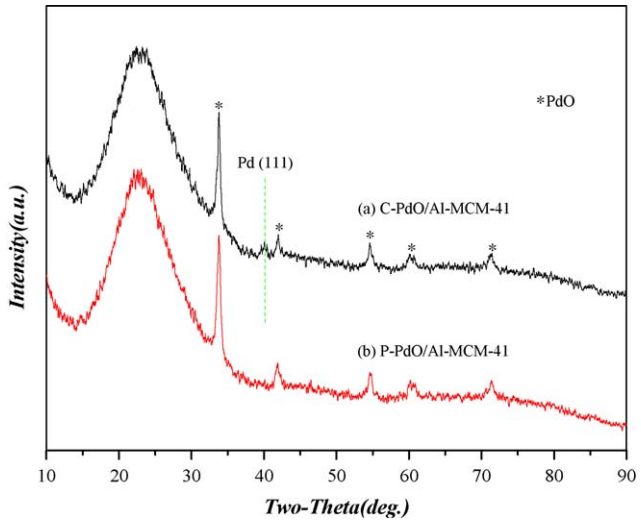

Fig. 9. The wide-angle XRD patterns of PdO/Al-MCM-41 catalysts after 48 h stability test: (a) C-PdO/Al-MCM-41 sample after 48 h reaction and (b) P-PdO/Al-MCM-41 sample after 48 h reaction.

A good dispersion of palladium oxide, giving an intimate contact with the support, leads to a stronger tendency for palladium to be oxidized and thus stabilizes palladium oxide against decomposition or reduction [44]. The stronger interaction between palladium oxide and molecular sieve support induced by plasma treatment can be directly verified by the CH_4-TPR characterization. As shown in Fig. 10, both the C-PdO/Al-MCM-41 and P-PdO/Al-MCM-41 catalysts exhibited only one reduction peak. The reduction peak for P-PdO/Al-MCM-41 catalyst (at 702 °C) was 27 °C higher than that for C-PdO/Al-MCM-41 counterpart (at 675 °C), suggesting a stronger interaction between palladium oxide and molecular sieve support.

To summarize, the deactivation of C-PdO/Al-MCM-41 catalyst was due to progressive reduction of the palladium oxide clusters. In other words, the improved stability observed on the P-PdO/Al-MCM-41 catalyst was closely related to the stronger interaction between palladium oxide and molecular sieve support. In addition, the sintering of PdO particles was insignificant during the stability test for both C-PdO/Al-MCM-41 and P-PdO/Al-MCM-41 catalysts.

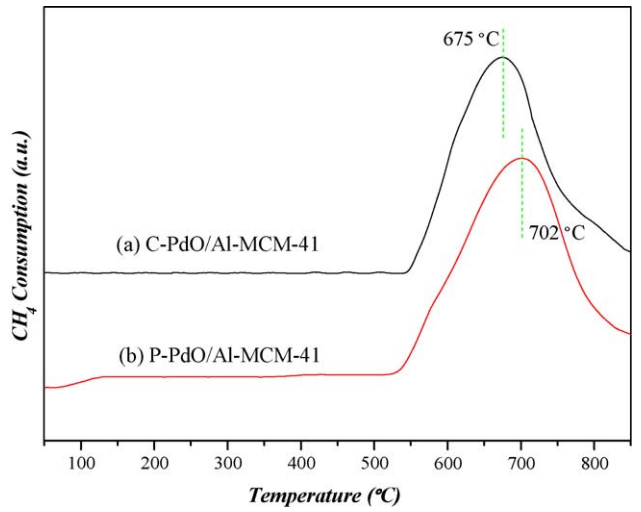

Fig. 10. CH_4-TPR profiles of (a) C-PdO/Al-MCM-41 and (b) P-PdO/Al-MCM-41 catalysts.

4. Conclusions

We employed the unique Al-MCM-41 as the model support to investigate the effect of glow discharge plasma treatment on the catalytic performance of Pd-based catalysts in methane combustion. Catalytic reactions demonstrated that the plasma treated PdO/Al-MCM-41 catalyst exhibited an enhanced initial activity and improved stability in comparison with the untreated counterpart catalyst.

To elucidate the beneficial effect of plasma treatment, a series of characterization experiments were performed. Acidity analysis (NH_3-TPD and Py-IR) and dispersion assessment (HR-TEM and XPS) techniques documented that the higher initial activity over plasma treated Pd-based catalyst was due to the enhanced acidity and an improved PdO dispersion. XRD and CH_4-TPR results proved that the enhanced stability of plasma treated Pd-based catalyst was closely related to the stronger interaction between palladium oxide and molecular sieve support. In addition, the sintering of PdO particles in our work was insignificant during the stability test.

Acknowledgments

The support from the National Natural Science Foundation of China (#20490203) and the instruments supplied by ABB Switzerland are greatly appreciated.

References

[1] E. Tzimpilis, N. Moschoudis, M. Stoukides, P. Bekiaroglou, Appl. Catal. B 84 (2008) 607–615.
[2] T.V. Choudhary, S. Banerjee, V.R. Choudhary, Appl. Catal. A 234 (2002) 1–23.
[3] Q. Liu, A.Q. Wang, X.H. Wang, P. Gao, X.D. Wang, T. Zhang, Micropor. Mesopor. Mater. 111 (2008) 323–333.
[4] O.R. Inderwildi, S.J. Jenkins, D.A. King, Angew. Chem. Int. Ed. 47 (2008) 5253–5255.
[5] J.G. McCarty, Nature 403 (2000) 35–36.
[6] V. Dupont, S.-H. Zhang, R. Bentley, A. Williams, Fuel 81 (2002) 799–810.
[7] P. Gélin, M. Primet, Appl. Catal. B 39 (2002) 1–37.
[8] C.-B. Wang, C.-M. Ho, H.-K. Lin, H.-C. Chiu, Fuel 81 (2002) 1883–1887.
[9] P.O. Thevenin, E. Pocoroba, L.J. Pettersson, H. Karhu, I.J. Väyrynen, S.G. Järås, J. Catal. 207 (2002) 139–149.
[10] Y.-X. Pan, C.-J. Liu, P. Shi, Appl. Surf. Sci. 254 (2008) 5587–5593.
[11] B. Stasinska, A. Machocki, K. Antoniak, M. Rotko, J.L. Figueiredo, F. Gonçalves, Catal. Today 137 (2008) 329–334.
[12] C.-J. Liu, K. Yu, Y.-P. Zhang, X. Zhu, F. He, B. Eliasson, Appl. Catal. B 47 (2004) 95–100.
[13] D. Cheng, K. Okumura, Y. Xie, C.-J. Liu, Appl. Surf. Sci. 254 (2007) 1506–1510.
[14] Y.-N. Li, Y.-B. Xie, C.-J. Liu, Catal. Lett. 125 (2008) 130–133.
[15] C.-J. Liu, G.P. Vissokov, B.W.-L. Jang, Catal. Today 72 (2002) 173–184.
[16] Z.-J. Wang, Y.-B. Xie, C.-J. Liu, J. Phys. Chem. C 112 (2008) 19818–19824.
[17] C.T. Kresge, M.E. Leonowicz, W.J. Roth, J.C. Vartuli, J.S. Beck, Nature 359 (1992) 710–712.
[18] D. Zhao, J. Feng, Q. Huo, N. Melosh, G.H. Fredrickson, B.F. Chmelka, G.D. Stucky, Science 279 (1998) 548–552.
[19] J.R.A. Sietsma, J.D. Meeldijk, M. Versluijs-Helder, A. Broersma, A.J. van Dillen, P.E. de Jongh, K.P. de Jong, Chem. Mater. 20 (2008) 2921–2931.
[20] R. Ryoo, S. Jun, J.M. Kim, M.J. Kim, Chem. Commun. (1997) 2225–2226.
[21] J.A.C. Ruiz, M.A. Fraga, H.O. Pastore, Appl. Catal. B 76 (2007) 115–122.
[22] M. Jia, A. Seifert, W.R. Thiel, Chem. Mater. 15 (2003) 2174–2180.
[23] X. Zhu, P. Huo, Y.-P. Zhang, D.-G. Cheng, C.-J. Liu, Appl. Catal. B 81 (2008) 132–140.
[24] Z.-J. Wang, Y. Zhao, L. Cui, H. Du, P. Yao, C.-J. Liu, Green Chem. 9 (2007) 554–559.
[25] S.J. Gregg, K.S.W. Sing, Adsorption, Surface Area and Porosity, 2nd ed., Academic Press, London, 1982.
[26] T. Kawabata, I. Atake, Y. Ohishi, T. Shishido, Y. Tian, K. Takaki, K. Takehira, Appl. Catal. B 66 (2006) 151–160.
[27] K.-L. Yu, C.-J. Liu, Y.-P. Zhang, F. He, X.-L. Zhu, B. Eliasson, Plasma Chem. Plasma Proc. 24 (2004) 393–403.
[28] O. M'Ramadj, D. Li, X. Wang, B. Zhang, G. Lu, Catal. Commun. 8 (2007) 880–884.
[29] L.M.T. Simplício, S.T. Brandão, E.A. Sales, L. Lietti, F. Bozon-Verduraz, Appl. Catal. B 63 (2006) 9–14.
[30] K. Persson, K. Jansson, S.G. Järås, J. Catal. 245 (2007) 401–414.
[31] C. Shi, L. Yang, J. Cai, Fuel 86 (2007) 106–112.
[32] W. Zhan, Y. Guo, Y. Wang, X. Liu, Y. Guo, Y. Wang, Z. Zhang, G. Lu, J. Phys. Chem. B 111 (2007) 12103–12110.
[33] E.P. Parry, J. Catal. 2 (1963) 371–379.
[34] K.-I. Fujimoto, F.H. Ribeiro, M. Avalos-Borja, E. Iglesia, J. Catal. 179 (1998) 431–442.

[35] O. Demoulin, G. Rupprechter, I. Seunier, B. Le Clef, M. Navez, P. Ruiz, J. Phys. Chem. B 109 (2005) 20454–20462.
[36] J.K. Lampert, M.S. Kazi, R.J. Farrauto, Appl. Catal. B 14 (1997) 211–223.
[37] D. Roth, P. Gélin, M. Primet, E. Tena, Appl. Catal. A 203 (2000) 37–45.
[38] P. Araya, S. Guerrero, J. Robertson, F.J. Gracia, Appl. Catal. A 283 (2005) 225–233.
[39] A. Baylet, S. Royer, P. Marécot, J.M. Tatibouët, D. Duprez, Appl. Catal. B 81 (2008) 88–96.
[40] H. Yoshida, T. Nakajima, Y. Yazawa, T. Hattori, Appl. Catal. B 71 (2007) 70–79.
[41] Y. Ozawa, Y. Tochihara, A. Watanabe, M. Nagai, S. Omi, Appl. Catal. A 259 (2004) 1–7.
[42] A. Baylet, S. Royer, P. Marécot, J.M. Tatibouët, D. Duprez, Appl. Catal. B 77 (2008) 237–247.
[43] T.V. Choudhary, S. Banerjee, V.R. Choudhary, Catal. Commun. 6 (2005) 97–100.
[44] C.A. Müller, M. Maciejewski, R.A. Koeppel, A. Baiker, J. Catal. 166 (1997) 36–43.